



Simultaneous Realization of High-Efficiency, Low-Drive Voltage, and Long Lifetime TADF OLEDs by Multifunctional Hole-Transporters

Journal:	<i>Journal of Materials Chemistry C</i>
Manuscript ID	TC-ART-01-2020-000330.R1
Article Type:	Paper
Date Submitted by the Author:	27-Mar-2020
Complete List of Authors:	Kamata, Takahiro; Yamagata University, Department of Organic Device Engineering Sasabe, Hisahiro; Yamagata univ., Organic Device Engineering Ito, Nozomi; Yamagata univ., Organic Device Engineering Sukegawa, Yoshihito; Yamagata univ., Organic Device Engineering Arai, Ayato; Yamagata univ., Organic Device Engineering Chiba, Takayuki; Yamagata University, Department of Organic Device Engineering Yokoyama, Daisuke; Yamagata University, Department of Organic Device Engineering, Graduate School of Science and Engineering Kido, Junji; Yamagata univ., Organic Device Engineering

Simultaneous Realization of High-Efficiency, Low-Drive Voltage, and Long Lifetime TADF OLEDs by Multifunctional Hole-Transporters

Takahiro Kamata, Hisahiro Sasabe, Nozomi Ito, Yoshihito Sukegawa, Ayato Arai, Takayuki Chiba, Daisuke Yokoyama, and Junji Kido**

Prof. H. Sasabe, T. Kamata, N. Ito, Y. Sukegawa, A. Arai, Prof. T. Chiba, Prof. D. Yokoyama, Prof. J. Kido
Department of Organic Materials Science
Yamagata University
4-3-16 Jonan, Yonezawa, Yamagata 992-8510, Japan
E-mail: h-sasabe@yz.yamagata-u.ac.jp;
kid@yz.yamagata-u.ac.jp

Prof. H. Sasabe, Prof. T. Chiba, Prof. D. Yokoyama, Prof. J. Kido
Research Center of Organic Electronics (ROEL), and Frontier Center for Organic Materials (FROM), Yamagata University
4-3-16 Jonan, Yonezawa, Yamagata 992-8510, Japan

Keywords: (thermally activated delayed fluorescence, long lifetime, hole-transporter, arylamine derivative, hexaphenylbenzene derivative)

Abstract: Although organic light emitting devices (OLEDs) based on thermally activated delayed fluorescence (TADF) have already realized impressively high external quantum efficiency (η_{ext}) of over 35%, their operation lifetime should still be improved for practical applications. In this study, we developed a molecular design for high triplet energy ($E_{\text{T}} = 2.7$ eV) multifunctional hole-transport layers (HTLs) based on a hexaphenylbenzene skeleton to realize record-breaking efficient and stable TADF OLEDs. By using a dibenzofuran-end-capped HTL named **4DBFHPB**, we could successfully develop a highly efficient, low-drive voltage, and stable green TADF OLED exhibiting η_{ext} of 19.2% and operation lifetime at 50% (LT_{50}) of ~24,000 h at an initial luminance of 1000 cd m⁻². The drive voltage at 1000 cd m⁻² was recorded to be 4.07 V. We also developed a sky-blue TADF OLED exhibiting η_{ext} of 21.5% and LT_{50} of ~1700 h at an initial luminance of 500 cd m⁻². The developed designs demonstrate record-breaking performances among the existing TADF OLEDs.

1. Introduction

Third generation organic light-emitting devices (OLEDs) based on thermally activated delayed fluorescent (TADF) emitters, which can achieve 100% electron-to-photon conversion using all the electrogenerated molecular excitons of singlets and triplets, are expected to be the next-generation low power consumption displays.^[1] After the breakthrough by Adachi and co-workers in 2012^[2], some research groups have reported ultra-high-efficiency TADF OLEDs with a maximum external quantum efficiency (η_{ext}) of 35%.^[3] Although TADF OLEDs have already achieved high efficiency, the operational lifetime still needs to be improved for their practical applications.^[4]

Similar to the second-generation phosphorescent OLEDs, neighboring materials such as host materials and carrier transport materials for the third-generation TADF OLEDs should have higher triplet energy (E_T) to suppress the quenching of triplet excitons than the emitter molecule because 75% of electrogenerated molecular triplet excitons contribute to boost the efficiency of OLEDs. Thus, high chemical stability, superior carrier transport ability, and high E_T are essential for high-performance phosphorescent and TADF OLEDs.^[5] In addition to these requirements, researchers should consider the potential exciplex formation with a TADF emitter because the lower-energy exciplex formation can induce the exciton quenching, causing inferior efficiency.^[4a,e,f] Unlike most phosphorescent emitters, TADF emitters, which consist of strong electron-donor and electron-acceptor units, can easily form an exciplex with carrier-transporters. As such, prolongation of the lifetime of TADF OLEDs becomes more difficult than their phosphorescent counterparts from the perspective of molecular design.

As an early example of green TADF OLEDs, in 2013, Nakanotani and Adachi have reported a (4s,6s)-2,4,5,6-tetra(9H-carbazol-9-yl)isophthalonitrile (**4CzIPN**)-based green TADF OLED with $\eta_{\text{ext},1000}$ of 14% and the operation lifetime at 50% (LT_{50}) of 2800 h at the initial luminance of 1000 cd m⁻².^[4a] They suggested that arylamine-based host materials are not suitable for the

green TADF emitter, **4CzIPN**; they produce low photoluminescent quantum yield (η_{PL}) due to the exciplex formation. In 2017, they significantly improved the efficiency and stability of the green TADF OLED by using a triazine-based n-type host material, **SF3-TRZ**. The **4CzIPN**-based green device showed $\eta_{\text{ext},1000}$ of 19.2% and LT_{50} of $\sim 10,000$ h at the initial luminance of 1000 cd m^{-2} .^[4d] Sasabe and Kido reported a highly efficient and long lifetime green TADF OLED based on **4CzIPN** with $\eta_{\text{ext},1000}$ of 21.6% and LT_{50} of $\sim 10,000$ h at the initial luminance of 1000 cd m^{-2} by using a hexaphenylbenzene (HPB)-based high E_{T} hole-transport layer (HTL), **4DBTHPB**.^[6] Note that **4DBTHPB** also plays a critical role in reducing the exciton quenching at the HTL and the emission layer (EML) interface and has high chemical stability toward electron carriers.

In this study, to formulate an effective molecular design strategy, we comprehensively investigated the thermal, photophysical properties, and hole-transport properties by using the Bässler disorder model and the device stability in a series of HPB derivatives with different end-cap groups. Consequently, these three HPB derivatives showed similar degree of horizontal orientation, however, dibenzofuran-end-capped **4DBFHPB** and **4DBFHPB** exhibited ~ 300 times higher hole mobility than **TATT** end-capped with phenyl units. **4DBFHPB** also achieved a **4CzIPN**-based green TADF OLED with $\eta_{\text{ext},1000}$ of 19.2% and long operation lifetime LT_{50} of 24,000 h at the initial luminance of 1000 cd m^{-2} . The drive voltage at 1000 cd m^{-2} was recorded to be 4.07 V. We also developed 2,3,4,5,6-pentakis(3,6-di-tert-butyl-9H-carbazol-9-yl)benzotrile (**5TCzBN**)-based sky-blue TADF OLED with high $\eta_{\text{ext,max}}$ of 21.5% and operation lifetime LT_{50} of 1700 h at the initial luminance of 500 cd m^{-2} . Our findings suggest that the operation lifetime of green and blue TADF OLEDs can be dramatically enhanced by using a sterically bulky hole-transporter with high chemical stability and high E_{T} .

2. Results and discussion

2.1. Molecular design and density functional theory calculation

To maximize the performance of TADF OLEDs, all molecular excitons of singlets and triplets should be confined. Therefore, we used high E_T components such as HPB as a core skeleton.^[7] HPB acts as a sterically bulky skeleton that can suppress exciton quenching caused by intermolecular interactions with the used emitter. Chemical stability of each material is essential to enhance the operation lifetime of TADF OLEDs. The stability of arylamine-based hole transporters is severely poor in the anion state, reducing the operation lifetime of OLEDs.^[8] In that case, the bond dissociation energy (BDE) of the materials should be considered for a long operation lifetime. The C–N bond of arylamine derivatives is significantly weak in the anion state, and its chemical degradation is one of the main reasons for the shorter operation lifetime of OLEDs. The BDE of the C–N bond of arylamine derivatives is reportedly improved by the introduction of dibenzothiophene (DBT) or dibenzofuran (DBF) moieties.^[5a,9] A sterically bulky HTL containing DBT or DBF moieties can be expected to improve the performance of TADF OLEDs.

To investigate the effect of the end-cap groups toward optoelectronic properties and the OLED performance, we compared three types of HPB derivatives end-capped with phenyl (**TATT**),^[7] DBT (**4DBTHPB**),^[6] and DBF (**4DBFHPB**) (**Figure 1**). First, density functional theory (DFT) calculations were conducted. Optimized structures were calculated at the RB3LYP 6-31G(d) level of theory for the ground states. The single-point energies were calculated at the RB3LYP 6-311+G(d,p) level of theory. Time-dependent DFT (TD-DFT) calculations for the singlet and triplet energies (E_S and E_T , respectively) were performed at the RB3LYP 6-31G(d) level of theory. The HOMO is located on the triarylamine moieties for all the derivatives, whereas the LUMO is located on the HPB skeleton for **TATT**, dibenzothiophen moieties for **4DBTHPB**, and dibenzofuran moieties for **4DBFHPB**. All the molecules have high E_T over 2.8 eV resulting in the sufficient confinement of triplet excitons for green and sky blue TADF emitters. Further, we conducted DFT calculations at the URB3LYP 6-31G(d) level of theory to evaluate the BDEs

for the anion states of three HPB-based HTLs. The BDE of **4DBFHPB** (1.80 eV) was calculated to be slightly higher than that of **4DBTHPB** (1.77 eV), and significantly higher than that of **TATT** (1.52 eV) (**Figure S1**).

2.2. Synthesis and thermal and physical properties

The synthetic route of the target material is shown in **Scheme S1**. **4DBFHPB** was synthesized via the Buchwald–Hartwig amination reactions of N-phenyldibenzo[*b,d*]furan-4-amine with 4,4''-dibromophenyl-2',3',5',6'-tetraphenyl-*p*-terphenyl with 54% yield. The material was characterized using ¹H-NMR spectroscopy, ¹³C-NMR spectroscopy, mass spectrometry, and elemental analysis. The materials were purified by train sublimation, and the purities were confirmed to be greater than 99.5% by high-performance liquid chromatography (HPLC).

The thermal properties of the material were estimated using differential scanning calorimetry (DSC) and thermogravimetric analysis (TGA). **4DBFHPB** showed a high glass transition temperature (T_g) of 135 °C, high melting point (T_m) of 313 °C, and high decomposition temperature (T_{d5}) of 490 °C. These parameters indicate the high thermal stability of the material. The optical properties were then evaluated using photoelectron yield spectroscopy (PYS) for the ionization potential (I_p),^[10] ultraviolet-visible (UV-Vis) absorption spectroscopy for the energy gap (E_g), and photoluminescence (PL) spectroscopy (**Figure S2**). **4DBFHPB** exhibited a wide E_g of 3.2 eV as estimated from the UV-Vis absorption edge and a deep I_p of -5.8 eV. By subtracting E_g from I_p , the electron affinities (E_a) were estimated to be -2.6 eV. The material exhibited a high E_T of 2.7 eV as estimated from the onset of the phosphorescent spectra at 5 K (**Figure S3**). This E_T value is sufficiently high to confine the triplet exciton on green and sky-blue TADF emitters.

2.3. Hole mobilities and molecular orientation

To evaluate the hole mobilities (μ_h) of HPB derivatives, we carried out time-of-flight (TOF) measurements of the HPB derivatives. The device structure was [Indium tin oxide (ITO, 100 nm)/HTL/Al (20 nm)], and the sample thickness was 5.5 μm for **TATT**, 5.3 μm for **4DBTHPB**, and 7.4 μm for **4DBFHPB**. **Figure 3** displays the representative transient TOF of the holes measured at room temperature. The μ_{hs} value was $1.5 \times 10^{-3} \text{ cm}^2 \text{ V}^{-1} \text{ s}^{-1}$ for **4DBTHPB** and $1.5 \times 10^{-3} \text{ cm}^2 \text{ V}^{-1} \text{ s}^{-1}$ for **4DBFHPB** at the electric field of $5.6 \times 10^{-5} \text{ V cm}^{-1}$ (**Figure 4**). These values are 300 times higher than that of **TATT** ($\mu_h = 5.0 \times 10^{-6} \text{ cm}^2 \text{ V}^{-1} \text{ s}^{-1}$). Because **4DBXHPB** derivatives showed unexpectedly higher μ_{hs} , we further investigated the temperature and field dependence of μ_{hs} by using the Bässler's disorder formalism to obtain more insight into the origin of hole-transporting properties.^[11]

To extract the hole-transport parameters, the temperature and field dependences were investigated using the TOF method (**Figure 5**). The energetic disorder (σ) and positional disorder (Σ) were also analyzed. Monté Carlo simulations yielded the temperature and field dependences of μ as follows:

For $\Sigma \geq 1.5$,

$$\mu = \mu_0 \exp\left[-\left(\frac{2\sigma}{3k_B T}\right)^2\right] \exp\left\{C\left[\left(\frac{\sigma}{k_B T}\right)^2 - \Sigma^2\right]\sqrt{E}\right\} \quad (1)$$

For $\Sigma < 1.5$,

$$\mu = \mu_0 \exp\left[-\left(\frac{2\sigma}{3k_B T}\right)^2\right] \exp\left\{C\left[\left(\frac{\sigma}{k_B T}\right)^2 - 2.25\right]\sqrt{E}\right\} \quad (2)$$

where μ_0 is the hypothetical mobility in the disorder-free system, k_B is Boltzmann's constant, E is the electric field, T is the temperature, and C is an empirical constant. The hole transport parameters μ_0 and σ were obtained by plotting $\log(\mu(E=0))$ against $(1000/T)^2$ (**Figure S4**). The

positional disorder parameters Σ and the values of C were obtained from the extrapolation of the slope of the plot of β versus $(\sigma/k_B T)^2$, where $\beta = C[(\sigma/k_B T)^2 - \Sigma^2]$ (**Figure S5**).

The energetic disorder σ is the fluctuation of the hopping site energy and shows both intramolecular and intermolecular contributions. In this case, the σ values had similar order to that of the standard deviation for the density-of-states distribution (~ 100 meV),^[12] and decreased in the order of **TATT** (96 meV) = **4DBFHPB** (96 meV) > **4DBTHPB** (79 meV).

The positional disorder Σ describes the fluctuation of the intermolecular distance and $\Sigma = 2.38$ for **TATT** and $\Sigma < 1.5$ for **4DBXHPB**. Considering that **4DBXHPB** derivatives had a much larger μ_0 of order 10^{-2} cm²/Vs, the intermolecular distance can be shortened and/or the well-ordered molecular orientations can be given in the vacuum-deposited film.

To further investigate the origin of the greater μ_h , we examined the molecular orientation by using variable-angle spectroscopic ellipsometry (VASE). Using VASE, we analyzed the order parameter S_{VASE} (**Figure 6**),^[13] which can be calculated based on the orientation of the transition dipole moments in organic films as follows:

$$S_{\text{VASE}} = \frac{3\langle \cos^2 \theta \rangle - 1}{2} = \frac{k_e^{\max} - k_o^{\max}}{k_e^{\max} + 2k_o^{\max}}, \quad (3)$$

where $\langle \dots \rangle$ indicates the ensemble average, θ is the angle between the axis of the transition dipole moment and the direction vertical to the substrate surface, and k_o^{\max} and k_e^{\max} are the ordinary and extraordinary extinction coefficients at the band peaks attributed to the transition dipole moment, respectively. We quantified the degree of orientation using S_{VASE} , which was 0 when the transition dipole moments of the molecules were completely random and -0.5 when they exhibited a completely horizontal orientation. As a result, all these HPB derivatives showed a similar degree of horizontal orientation with S_{VASE} of around -0.15 (see Table 1). This results indicate that the introduction of larger π -planes such as DBF or DBT into the

end-cap groups does not highly influence the horizontal molecular orientation due to the significantly bulky HPB core skeleton. Therefore, a significant increase in μ_h compared to the benchmark material, **TATT** with smaller end-cap groups, can be attributed to the shortened intermolecular distance between HOMOs in **4DBXHPB** derivatives.

2.4. Green TADF OLED performance

As discussed in Section 1, the lifetime (LT_{50}) of green TADF is improving and reaching $\sim 10,000$ h at the brightness value of 1000 cd cm^{-2} ; however, it must be further improved for practical applications. To evaluate the performance of the novel HTL, OLED devices based on **4CzIPN** were fabricated with the structure of [ITO (100 nm)/triphenylamine-containing polymer: 4-isopropyl-4-methyldiphenyl-iodonium tetrakis(pentafluorophenyl)borate (**PPBI**)^[14] (20 nm)/N,N'-di(1-naphthyl)-N,N'-diphenyl-(1,1'-biphenyl)-4,4'-diamine (**NPD**) (10 nm)/HTL (10 nm)/**mCBP**^[15]: 20 wt% **4CzIPN** (30 nm)/**DBT-TRZ**^[16] (10 nm)/1,4-di(1,10-phenanthrorin-2-yl)benzene (**DPB**)^[17]: 20 wt% 8-quinolinolato lithium (**Liq**) (40 nm)/2-(2',2''-bipyridine-6'-yl)phenolate (**Libpp**)^[18] (1 nm)/Al]. We used **DBT-TRZ** as the hole-blocking layer and **Liq**-doped **DPB** as the ETL to obtain long operation stability (**Figure 7**). Moreover, **Libpp** was used for the electron-injection layer to realize a low driving voltage. **NPD** was used between the polymer buffer layer and HTL for a stepwise hole injection.^[19] All the devices showed high $\eta_{\text{ext},1000}$ of 19–21% at the brightness of 1000 cd m^{-2} . **4DBTHPB**- and **4DBFHPB**-based devices exhibited lower turn-on voltage of 2.5 V at 1 cd m^{-2} (V_{on}) than the **TATT**-based device ($V_{\text{on}} = 2.7 \text{ V}$) (**Figure 8**). At the brightness of 1000 cd m^{-2} , **4DBTHPB**- and **4DBFHPB**-based devices also exhibited very low drive voltage of 4.0 V and high $\eta_{\text{p},1000}$ of over 52 lm W^{-1} . Then, we evaluated the stability of green TADF OLEDs. **Figure 8(c)** shows the normalized luminance as a function of the operation time at the current density of 10 mA cm^{-2} , which corresponds to the luminance of $\sim 6000 \text{ cd m}^{-2}$. The operation lifetime at 50% of the initial

luminance (LT_{50}) at the constant current density of 10 mA cm^{-2} was 497 h for **4DBFHPB**, 419 h for **4DBTHPB**, and 356 h for **TATT**. Dibenzofuran or dibenzothiphen end-capped HTLs (**4DBFHPB** and **4DBTHPB**) exhibited much longer lifetime than their phenyl counterpart (**TATT**) due to the superior stability of the anion state and their higher mobility.

We then carried out the acceleration test at the constant current density of 20 and 30 mA cm^{-2} . The operation lifetime at the initial luminance (L_0) of 1000 cd m^{-2} was estimated by these luminance acceleration tests based on the formula $L_0^n \times LT(L_0) = \text{const.}$ ^[20] Consequently, the **4DBFHPB**-based device exhibited an operation lifetime of $LT_{50} = 24,000 \text{ h}$, which is 2.4 times longer than that of the state-of-the-art TADF OLEDs.^[4,6] The **4DBTHPB**-based device also showed a long operation lifetime of $LT_{50} = 20,000 \text{ h}$, which is approximately twice that of **TATT** ($LT_{50} = 12,000 \text{ h}$). All the OLED performances are summarized in **Table 3**. The obtained lifetimes are the longest among the TADF OLEDs, and more than twice longer than OLED performances. The operating voltages are also lower than that of the state-of-the-art green OLEDs (**Table 4**).

To get deeper insights into the lifetime, we investigated the location of the emission zone. For this, we made three types of devices with different doping ratio of **4CzIPN** (10, 15, and 20 wt%) inserted 3 nm rubrene as a quencher between HTL/EML interface (**Figure S6**). The devices with rubrene showed significantly lower η_{ext} s compared with the devices without rubrene, and the higher doping ratio of **4CzIPN** caused the much lower η_{ext} s. These results apparently indicate that the emission zone is located near at HTL/EML interface, especially at low luminance region. Thus, the stability in the anion state is crucially important for HTL to prolong the lifetime in this device configuration. Further, we made hole-only devices with the structure of [ITO /triphenylamine-containing polymer : PPBI (20 nm) (20 nm) /NPD (10 nm) /HTL (10 nm) /mCBP: 20wt% 4CzIPN (30 nm) /NPD (40 nm) /Al (100 nm)] to differentiate three HTLs (**Figure S7**). As shown in the J - V characteristics, the current densities of **4DBFHPB** and **4DBTHPB** were similar, and higher than that of **TATT**. These results indicate

that the recombination zones of **4DBFHPB** and **4DBFHPB** are similar, and farer from the HTL/EML interface than that of **TATT**.

2.5. Sky-blue TADF OLED performances

Compared to green TADF OLEDs, research on the stability of blue TADF OLEDs is limited due to the small number of available materials.^[1c] As a proof-of-concept, we tested our HTLs for the sky-blue TADF emitter, **5TCzBN**,^[21] instead of **4CzIPN** in the same OLED architecture (**Figure 7**). Here, we used 30 nm of **mCBP**: 30 wt% **5TCzBN** as an EML. The **4DBFHPB**-based device exhibited a lower V_{1000} of 3.9 V than the **TATT**-based device ($V_{1000} = 4.2$ V) (**Figure 5**). The **4DBFHPB**-based device also exhibited high $\eta_{p,1000}$ of 36 lm W⁻¹, $\eta_{ext,1000}$ of 17.3% and $\eta_{ext,max}$ of 21.5%.

Then, we evaluated the stability of the sky-blue TADF OLEDs. **Figure 9(c)** shows the normalized luminance as a function of operation time at the current density of 3 mA cm⁻², which corresponds to the luminance of ~1250 cd m⁻². The operation lifetime at the initial luminance (L_0) of 500 cd m⁻² was estimated using the luminance acceleration test. The **4DBFHPB**-based device exhibited a longer operation lifetime at 50% of the initial luminance ($LT_{50} = 1,700$ h) than **4DBTHPB**- ($LT_{50} = 1,100$ h) and **TATT**-based ($LT_{50} = 1,000$ h) devices. Note that this value is the best one among the sky-blue TADF OLEDs, and it is approximately twice the operation lifetime of the reported value (**Table 5**).^[21,22] All device performances are summarized in **Table 3**.

As mentioned in green TADF OLEDs, HTL is reportedly unstable toward anion state, and one of the most important factors to limit the device lifetime. In this context, superior BDE, higher hole-mobility and injection property of **4DBFHPB** are the important factors to prolong the lifetimes even in blue TADF OLEDs.

3. Conclusion

In this study, we investigated the interface between the hole transport layer and the emission layer to prolong the lifetime of TADF OLEDs, where (i) chemical instability of the hole transport layer can reduce the lifetime of OLEDs, and (ii) significant quenching of molecular excitons can occur due to the low-band-gap exciplex formation between the TADF emitter and the hole-transporter. To solve these critical problems, we developed a novel multifunctional hole-transporter named **4DBFHPB** containing a hexaphenylbenzene skeleton and dibenzofuran end-cap groups with high chemical stability toward the anion state, deep I_p of -5.8 eV, high E_T of 2.7 eV, and μ_{th} of order 10^{-3} $\text{cm}^2 \text{V}^{-1} \text{s}^{-2}$, which is 300 times greater than that with its phenyl counterpart. The large BDE increases the stability toward the anion, and the deep I_p and high E_T can reduce the exciplex formation suppressing the quenching of molecular excitons. We investigated the substitution effect of hexaphenylbenzene-based hole-transporters on the device performance of TADF OLEDs and found that hole-transporters with dibenzofuran and dibenzothiophene end-capping groups significantly prolong the lifetime of TADF OLEDs compared to phenyl end-capping groups. By using **4DBFHPB**, we successfully realized a highly efficient and stable green TADF OLED exhibiting $\eta_{\text{ext},1000}$ of 19.2% and LT_{50} of $\sim 24,000$ h at the initial luminance of $1,000 \text{ cd m}^{-2}$. We also obtained a highly efficient and stable sky-blue TADF OLED exhibiting $\eta_{\text{ext,max}}$ of 21.5% and LT_{50} of ~ 1700 h at the initial luminance of 500 cd m^{-2} by using **4DBFHPB**. These values are twice the operation lifetime of the state-of-the-art TADF OLEDs. The molecular design strategy demonstrated in this work will contribute to promoting the commercialization of TADF OLEDs.

4. Experimental Section

General considerations:

Quantum chemical calculations were performed using the hybrid density functional theory (DFT), functional Becke and Hartree-Fock exchange, and Lee Yang and Parr correlation (B3LYP) as implemented in the Gaussian 09 program packages.^[23] Electrons were described

by the Pople 6-31G(d,p) and 6-311+G(d,p) basis sets for molecular structure optimization and single-point energy calculations, respectively. The BDEs of the anion states were calculated at the URB3LYP 6-31G(d) level of theory according to the enthalpy change in the corresponding reaction of homolytic cleavage of a single bond in the gas phase at 298 K and 1 atm.^[24] ¹H-NMR and ¹³C-NMR spectra were recorded on a JEOL 400 spectrometer. Mass spectra were obtained using a JEOL JMS-K9 mass spectrometer and a Waters SQD2 mass spectrometer with atmospheric pressure solid analysis probe (ASAP). Differential scanning calorimetry (DSC) was performed using a Perkin-Elmer Diamond DSC Pyris instrument under nitrogen atmosphere at a heating rate of 10°C min⁻¹. Thermogravimetric analysis (TGA) was undertaken using a SEIKO EXSTAR 6000 TG/DTA 6200 unit under nitrogen atmosphere at a heating rate of 10°C min⁻¹. UV-Vis spectra were measured using a Shimadzu UV-3150 UV-vis-NIR spectrophotometer. Photoluminescence spectra were measured using a FluroMax-2 (Jobin-Yvon-Spex) luminescence spectrometer. The ionization potential (I_p) was determined using a photoelectron yield spectroscopy (PYS) in vacuum ($\sim 10^{-3}$ Pa).^[10] The phosphorescent spectra were measured using a streak camera (C4334 from Hamamatsu Photonics) at 5K.

Synthesis of 4DBFHPB:

4,4'-Dibromo-2',3',5',6'-tetraphenyl-*p*-terphenyl (0.69 g, 1.0 mmol), *N*-phenyldibenzo[*b,d*]furan-4-amine (0.55g, 2.0 mmol), and sodium-*t*-butoxide (0.5 g, 5.2 mmol) were added to a round bottom flask. Next, dry toluene (10 mL) was added to the mixture, and nitrogen (N₂) bubbled through the mixture for 1 h. Then, Pd₂(dba)₃ (0.092 g, 0.10 mmol) and tris-*t*-butylphosphonium tetrafluoroborate (0.058 g, 0.2 mmol) were added and the resultant mixture was stirred for 1.5 h at reflux temperature under the N₂ flow. The mixture was filtered through the silica gel pad and evaporated to dryness. The resulting solid was purified by chromatography on the silica gel (eluent: CH₂Cl₂/hexane = 2/3 v/v) to afford **4DBFHPB** (0.57 g, 54 %) as a white solid: ¹H-NMR (400 MHz, CDCl₃, δ): 7.90 (d, $J = 7.3$ Hz, 2H), 7.63–7.65

(m, 2H), 7.38–7.42 (m, 2H), 7.28–7.34 (m, 4H), 7.12–7.20 (m, 6H), 6.84–6.95 (m, 24H), 6.78–6.80 (m, 4H), 6.70 (d, $J = 8.7$ Hz, 4H), 6.63 (d, $J = 8.7$ Hz, 4H); ^{13}C -NMR (100 MHz, CDCl_3 , δ): 156.00, 150.34, 147.48, 144.26, 140.85, 140.45, 140.31, 136.01, 132.28, 132.15, 131.70, 128.90, 127.05, 126.77, 126.00, 125.29, 124.35, 124.29, 123.52, 122.77, 122.52, 122.33, 122.03, 120.62, 115.98, 112.18, 77.48, 77.16, 76.84 ppm; MS: m/z 1049.7 $[\text{M}]^+$; Elemental analysis (%) calculated for $\text{C}_{78}\text{H}_{52}\text{N}_2\text{O}_2$: C 89.29, H 5.00, N 2.67 %; found: C 89.41, H 4.72, N 2.63.

Device Fabrication and Characterization:

NPD and **Liq** were purchased from e-Ray Optoelectronics Technology Co., Ltd. **mCBP**^[15], **4CzIPN**^[22], **5TCzBN**^[21], **DBT-TRZ**^[16a], **DPB**^[17a], and **Libpp**^[18] were prepared according to the previous reports. The HPLC purities for HTLs were 99.8% for **TATT** (THF/ CH_3CN / H_2O = 6/1/3 (vol)), 99.3% for **4DBTHPB** (THF/ CH_3CN = 1/9 (vol)), 100% for **4DBFHPB** (THF/ CH_3CN = 1/9 (vol)). All organic materials were purified by temperature gradient sublimation in vacuum. The substrates were cleaned with ultra-purified water and organic solvents (acetone and then isopropanol), and then dry-cleaned for 30 min by exposure to UV-ozone. The organic layers were deposited onto the ITO substrate in vacuum (ca. 10^{-5} Pa) successively. Al was patterned using a shadow mask with an array of 2 mm \times 2 mm openings without breaking the vacuum (ca. 10^{-5} Pa). The EL spectra were taken using an optical multichannel analyzer Hamamatsu Photonics PMA-11. The current density–voltage and luminance–voltage characteristics were measured using a Keithley source measure unit 2400 and a Minolta CS200 luminance meter, respectively.

Acknowledgements

This study was partially supported by JSPS KAKENHI (17H03131) from JSPS, and by the Center of Innovations (COI) Program from Japan Science and Technology Agency (JST).

References

- [1] a) C. Adachi, *Jpn. J. Appl. Phys.* **2014**, *53*, 060101; b) Z. Yang, Z. Mao, Z. Xie, Y. Zhang, S. Liu, J. Zhao, J. Xu, Z. Chi, M. P. Aldred, *Chem. Soc. Rev.* **2017**, *46*, 915; c) Y. Im, M. Kim, Y. J. Cho, J.-A. Seo, K. S. Yook, J. Y. Lee, *Chem. Mater.* **2017**, *29*, 1946; d) M. Y. Wong, E. Z.-Colman, *Adv. Mater.* **2017**, *29*, 1605444; e) R. Komatsu, H. Sasabe, J. Kido, *J. Phon. Ener.* **2018**, *8*, 032108.
- [2] H. Uoyama, K. Goushi, K. Shizu, H. Nomura, C. Adachi, *Nature* **2012**, *492*, 234.
- [3] a) H. Kaji, H. Suzuki, T. Fukushima, K. Shizu, K. Suzuki, S. Kubo, T. Komino, H. Oiwa, F. Suzuki, A. Wakamiya, Y. Murata, C. Adachi, *Nat. Commun.* **2015**, *6*, 8476; c) T.-A. Lin, T. Chatterjee, W.-L. Tsai, W.-K. Lee, M.-J. Wu, M. Jiao, K.-C. Pan, C.-L. Yi, C.-L. Chung, K.-T. Wong, C.-C. Wu, *Adv. Mater.* **2016**, *28*, 6976; d) C.-K. Moon, K. Suzuki, K. Shizu, C. Adachi, H. Kaji, J.-J. Kim, *Adv. Mater.* **2017**, *29*, 1606448; e) P. Rajamalli, N. Senthilkumar, P.-Y. Huang, C.-C. Ren-Wu, H.-W. Lin, C.-H. Cheng, *J. Am. Chem. Soc.* **2017**, *139*, 10948; f) P. L. dos Santos, J. S. Ward, D. G. Congrave, A. S. Batsanov, J. Eng, J. E. Stacey, T. J. Penfold, A. P. Monkman, M. R. Bryce, *Adv. Sci.* **2018**, *5*, 1700989; g) M. Liu, R. Komatsu, X. Cai, K. Hotta, S. Sato, K. Liu, D. Chen, Y. Kato, H. Sasabe, S. Ohisa, Y. Suzuri, D. Yokoyama, S.-J. Su, J. Kido, *Chem. Mater.* **2017**, *29*, 8630; h) T.-L. Wu, M.-J. Huang, C.-C. Lin, P.-Y. Huang, T.-Y. Chou, R.-W. Chen-Cheng, H.-W. Lin, R.-S. Liu, C.-H. Cheng, *Nat. Photonics* **2018**, *12*, 235; i) D. H. Ahn, S. W. Kim, H. Lee, I. J. Ko, D. Karthik, J. Yo. Lee, J. H. Kwon, *Nat. Photon.* **2019**, *13*, 540; j) Y. Kondo, K. Yoshiura, S. Kitera, H. Nishi, S. Oda, H. Gotoh, Y. Sasada, M. Yanai, T. Hatakeyama, *Nat. Photon.* **2019**, *13*, 678.
- [4] a) H. Nakanotani, K. Masui, J. Nishide, T. Shibata, C. Adachi, *Sci. Rep.* **2013**, *3*, 2127; b) T. Furukawa, H. Nakanotani, M. Inoue, C. Adachi, *Sci. Rep.* **2015**, *5*, 8429; c) Y. Im, W. Song, J. Y. Lee, *J. Mater. Chem. C* **2015**, *3*, 8061; d) L. S. Cui, S. B. Ruan, F. Bencheikh, R. Nagata, L. Zhang, K. Inada, H. Nakanotani, L. S. Liao, C. Adachi, *Nat*

- Commun* **2017**, *8*, 2250; e) X.-K. Liu, Z. Chen, C.-J. Zheng, C.-L. Liu, C.-S. Lee, F. Li, X.-M. Ou, X.-H. Zhang, *Adv. Mater.* **2015**, *27*, 2378; f) W. Liu, J.-X. Chen, C.-J. Zheng, K. Wang, D.-Y. Chen, F. Li, Y.-P. Dong, C.-S. Lee, X.-M. Ou, X.-H. Zhang, *Adv. Funct. Mater.* **2016**, *26*, 2002.
- [5] a) W. Song, J. Y. Lee, *Adv. Opt. Mater.* **2017**, 1600901; b) H. Sasabe, J. Kido, *Chem. Mater.* **2011**, *23*, 621; c) H. Sasabe, J. Kido, *J. Mater. Chem. C* **2013**, *1*, 1699.
- [6] T. Kamata, H. Sasabe, M. Igarashi, J. Kido, *Chem. Eur. J.* **2018**, *24*, 4590.
- [7] S. Watanabe, J. Kido, *Chem. Lett.* **2007**, *36*, 590.
- [8] a) D. Y. Kondakov, *J. Appl. Phys.* **2008**, *104*, 084520; b) S. Schmidbauer, A. Hohenleutner, B. König, *Adv. Mater.* **2013**, *25*, 2114.
- [9] a) H. Fukagawa, T. Shimizu, Y. Kiribayashi, Y. Osada, T. Kamada, T. Yamamoto, N. Shimidzu, T. Kurita, *Appl. Phys. Lett.* **2013**, *103*, 143306; b) H. Fukagawa, T. Shimizu, H. Kawano, S. Yui, T. Shinnai, A. Iwai, K. Tsuchiya, T. Yamamoto, *J. Phys. Chem. C* **2016**, *120*, 18748.
- [10] H. Ishii, D. Tsunami, T. Suenaga, N. Sato, Y. Kimura, M. Niwano, *J. Surf. Sci. Soc. Jpn.* **2007**, *28*, 264.
- [11] a) H. Bässler, *Phys. Status Solidi B* **1993**, *175*, 15; b) P. M. Borsenberger, D. S. Weiss, Eds. *Organic Photoreceptors for Imaging Systems*, Marcel Dekker Inc., New York, 1993.
- [12] V. Coropceanu, J. Cornil, D. A. da Silva Filho, Y. Olivier, R. Silbey, J.-L. Brédas, *Chem. Rev.* **2007**, *107*, 926.
- [13] D. Yokoyama, *J. Mater. Chem.* **2011**, *21*, 19187.
- [14] J. Kido, G. Harada, M. Komada, H. Shionoya, K. Nagai, *ACS. Synp. Ser.* **1997**, *672*, 381.
- [15] P. Shrögel, N. Langer, C. Schildknecht, G. Wagenblast, C. Lennartz, P. Strohriegl, *Org. Electron.* **2011**, *12*, 2047.

- [16] a) Y. Nagai, H. Sasabe, J. Takahashi, N. Onuma, T. Ito, S. Ohisa, J. Kido, *J. Mater. Chem. C* **2017**, *5*, 527; b) T. Ito, H. Sasabe, Y. Nagai, Y. Watanabe, N. Onuma, J. Kido, *Chem. Eur. J.* **2019**, *25*, 7308.
- [17] a) E. C. Riesgo, X. Jin, R. P. Thummel, *J. Org. Chem.* **1996**, *61*, 3017; b) Y.-J. Pu, G. Nakata, H. Satoh, H. Sasabe, D. Yokoyama, J. Kido, *Adv. Mater.* **2012**, *24*, 1765.
- [18] Y.-J. Pu, M. Miyamoto, K.-I. Nakayama, T. Oyama, Y. Masaaki, J. Kido, *Org. Electron.* **2009**, *10*, 228.
- [19] T. Matsushima, K. Goushi, C. Adachi, *Chem. Phys. Lett.* **2007**, *435*, 327.
- [20] C. Féry, B. Racine, D. Vaufrey, H. Doyeux, S. Cinà, *App. Phys. Lett.* **2005**, *87*, 213502.
- [21] D. Zhang, M. Cai, Y. Zhang, D. Zhang, L. Duan, *Mater. Horiz.* **2016**, *3*, 145.
- [22] D. Zhang, P. Wei, D. Zhang, L. Duan, *App. Mater. Interf.* **2017**, *9*, 19040.
- [23] *Gaussian 09*, Revision D.01, M. J. Frisch, G. W. Trucks, H. B. Schlegel, G. E. Scuseria, M. A. Robb, J. R. Cheeseman, G. Scalmani, V. Barone, B. Mennucci, G. A. Petersson, H. Nakatsuji, M. Caricato, X. Li, H. P. Hratchian, A. F. Izmaylov, J. Bloino, G. Zheng, J. L. Sonnenberg, M. Hada, M. Ehara, K. Toyota, R. Fukuda, J. Hasegawa, M. Ishida, T. Nakajima, Y. Honda, O. Kitao, H. Nakai, T. Vreven, J. A. Montgomery, Jr., J. E. Peralta, F. Ogliaro, M. Bearpark, J. J. Heyd, E. Brothers, K. N. Kudin, V. N. Staroverov, R. Kobayashi, J. Normand, K. Raghavachari, A. Rendell, J. C. Burant, S. S. Iyengar, J. Tomasi, M. Cossi, N. Rega, J. M. Millam, M. Klene, J. E. Knox, J. B. Cross, V. Bakken, C. Adamo, J. Jaramillo, R. Gomperts, R. E. Stratmann, O. Yazyev, A. J. Austin, R. Cammi, C. Pomelli, J. W. Ochterski, R. L. Martin, K. Morokuma, V. G. Zakrzewski, G. A. Voth, P. Salvador, J. J. Dannenberg, S. Dapprich, A. D. Daniels, Ö. Farkas, J. B. Foresman, J. V. Ortiz, J. Cioslowski, and D. J. Fox, Gaussian, Inc., Wallingford CT, 2013.
- [24] (a) N. Lin, J. Qiao, L. Duan, L. Wang, Y. Qiu, *J. Phys. Chem. C* **2014**, *118*, 7569. M. Hong, M. K. Ravva, R. Winget, J.-L. Bredas, *Chem. Mater.* **2016**, *28*, 5791.

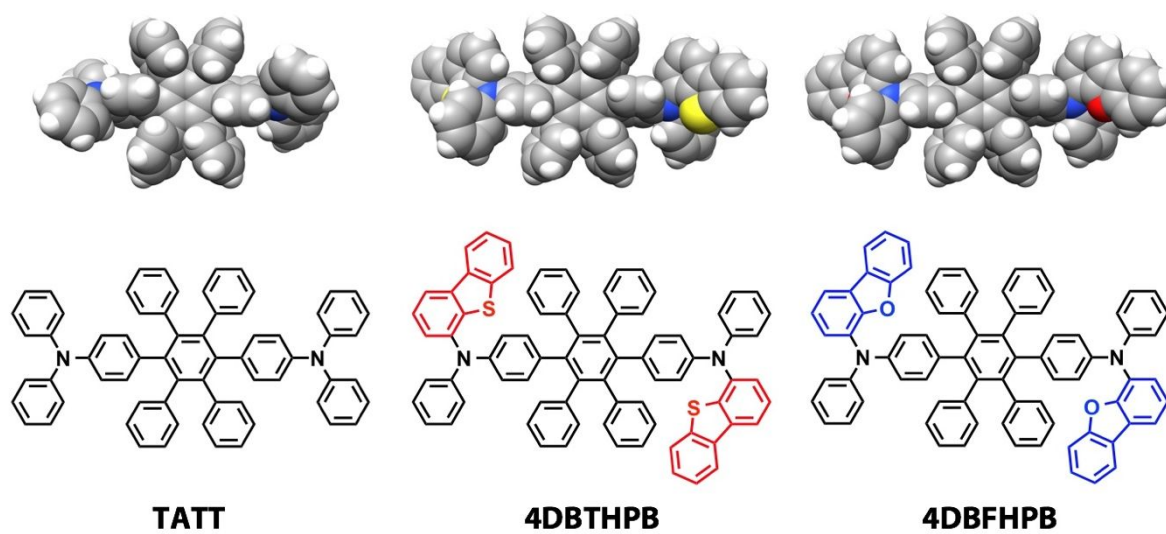


Figure 1. Chemical structures of HTLs used in this study.

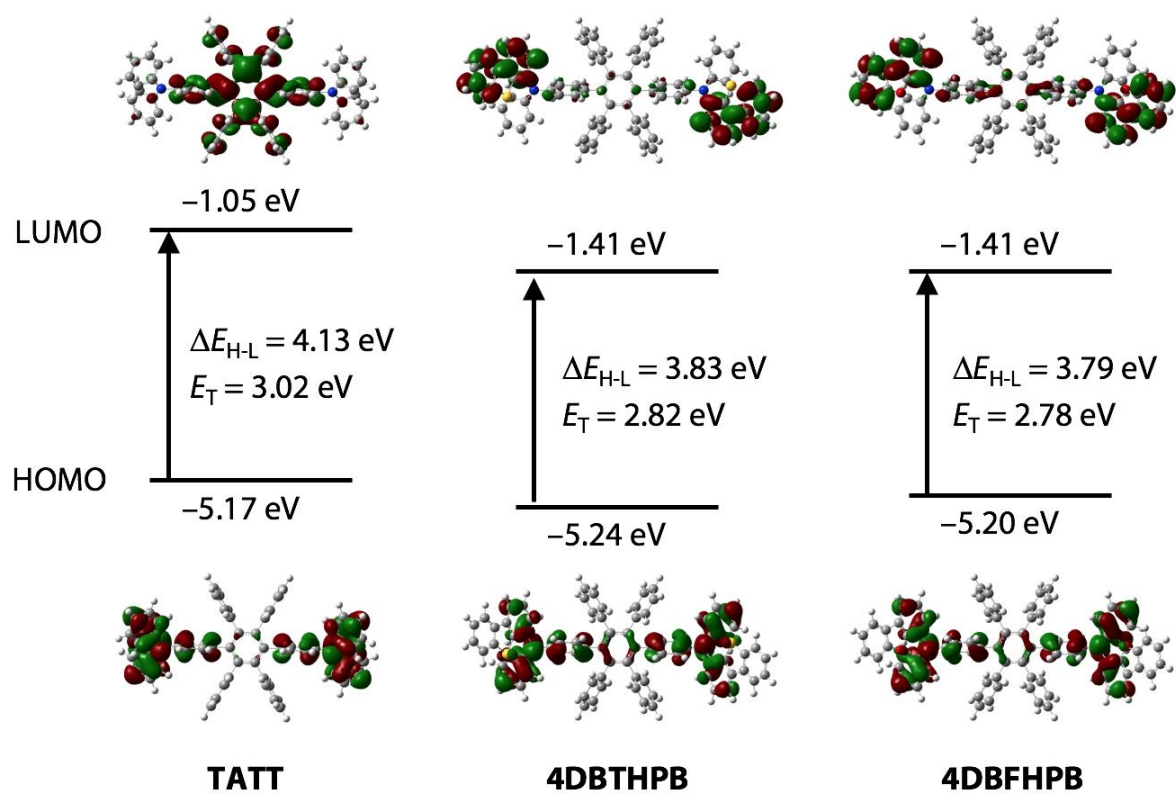


Figure 2. HOMO and LUMO distributions and energy levels, HOMO–LUMO energy differences (ΔE_{H-L}), and the lowest triplet energy (E_T) for HTLs used in this study.

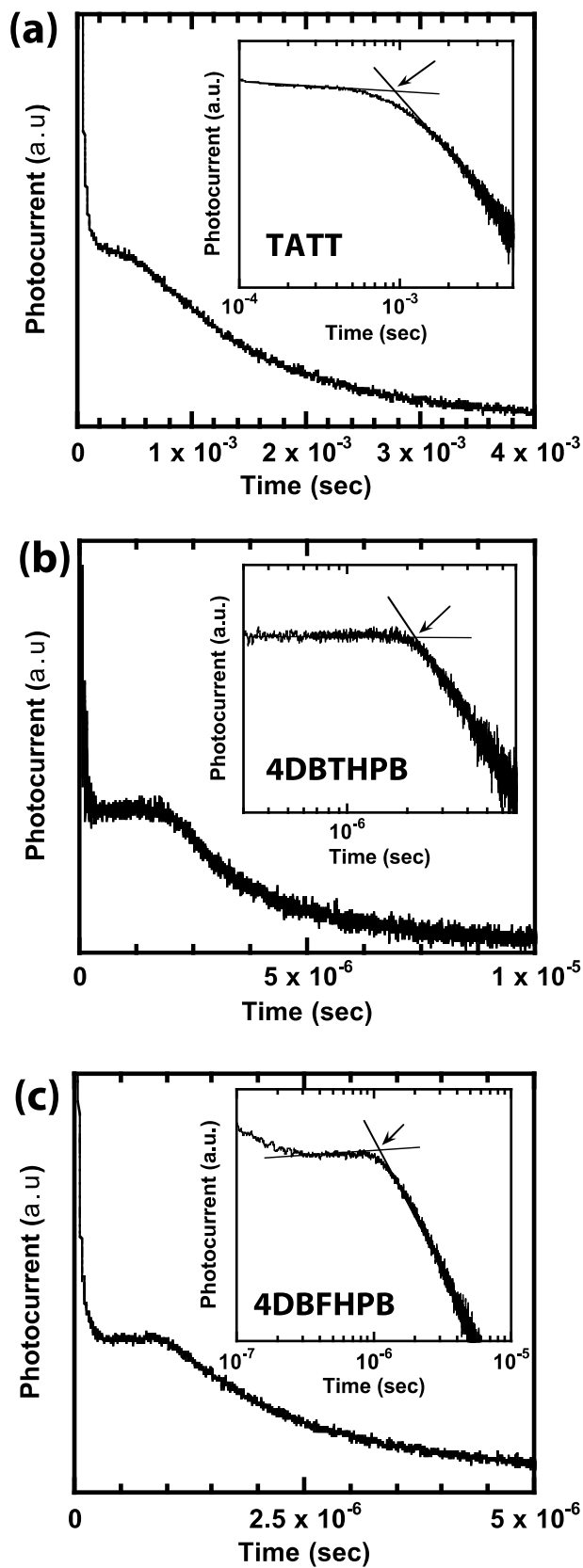


Figure 3. Representative TOF transients for holes at room temperature: a) TATT at $E = 2.5 \times 10^5 \text{ V cm}^{-1}$, b) 4DBTHPB at $E = 2.5 \times 10^5 \text{ V cm}^{-1}$, c) 4DBFHPB at $E = 4.9 \times 10^5 \text{ V cm}^{-1}$.

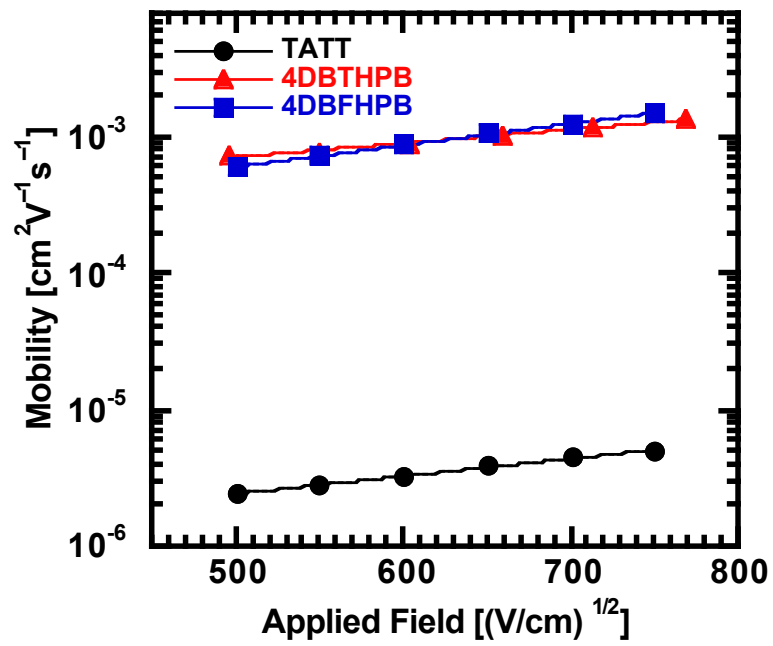


Figure 4. Hole mobilities plotted with respect to $E^{1/2}$ for HPB derivatives.

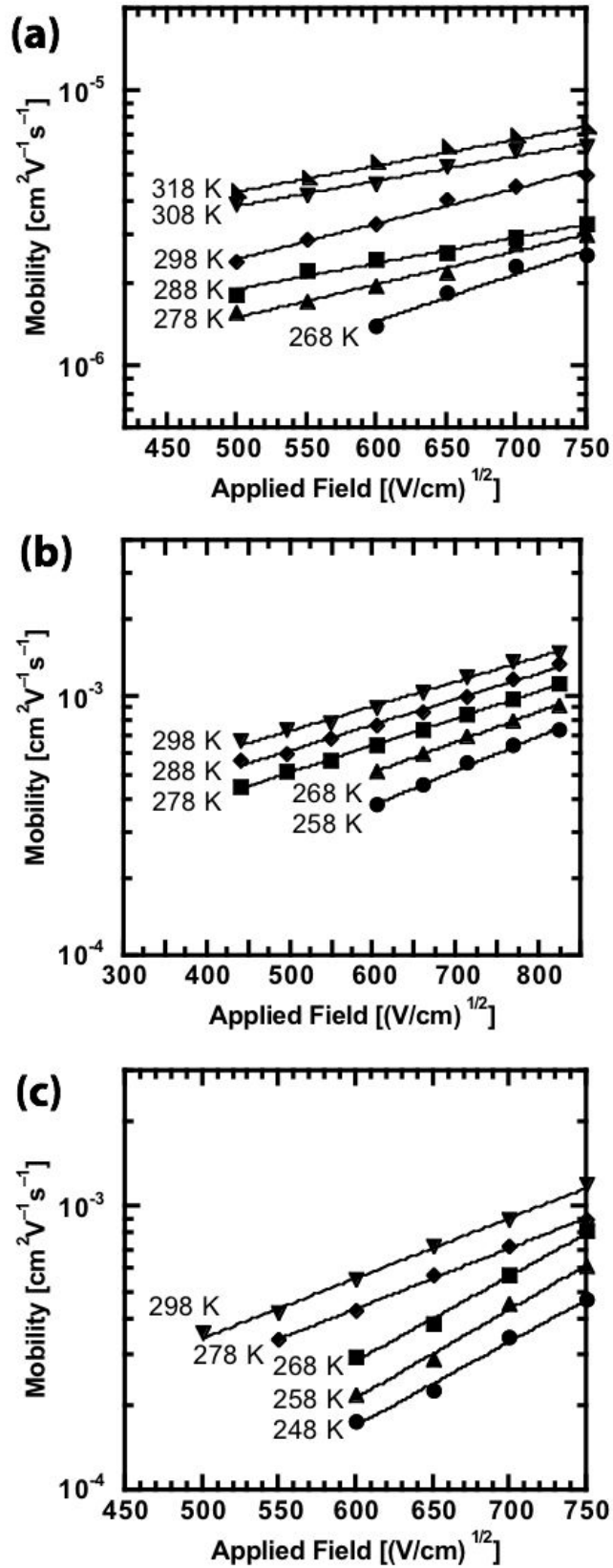


Figure 5. The temperature dependence of field-dependent mobility: a) TATT, b) 4DBTHPB, c) 4DBFHPB.

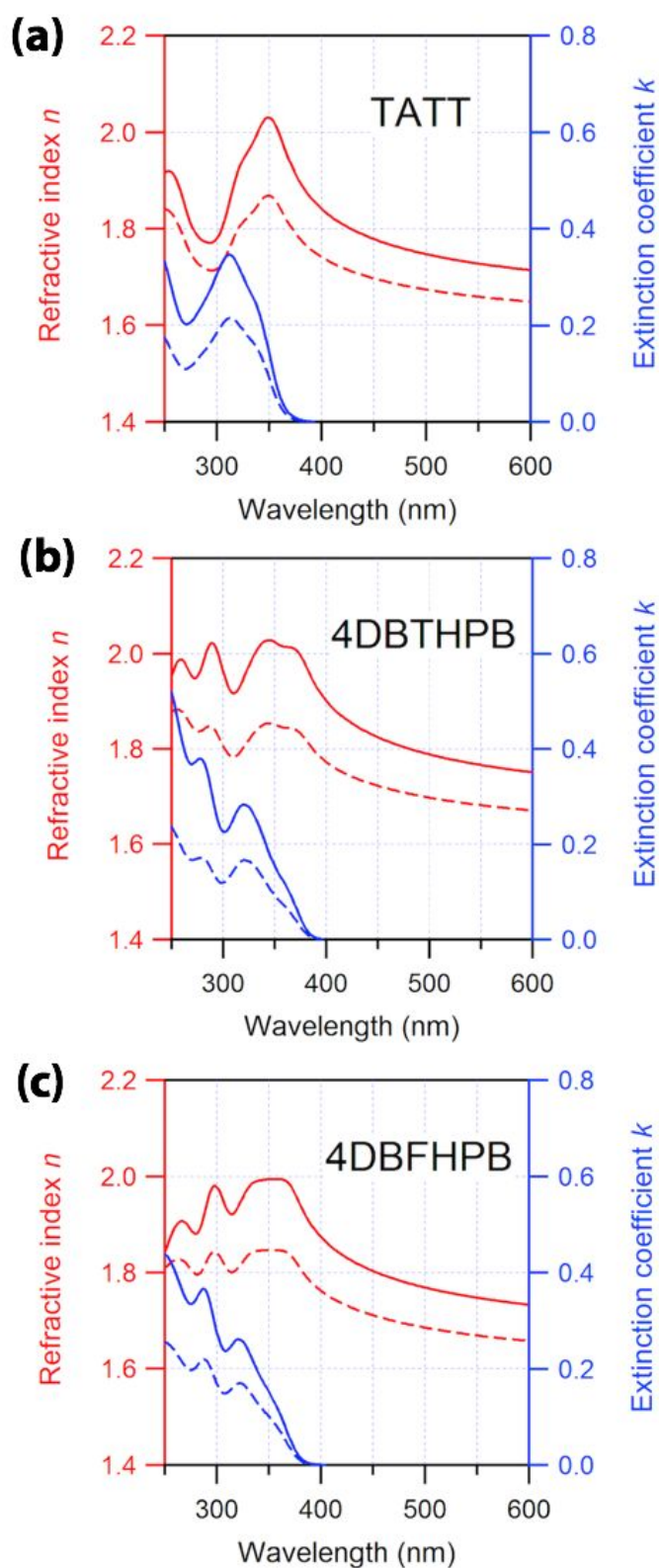


Figure 6. Anisotropies of the refractive indices and extinction coefficients of (a) **TATT**, (b) **4DBTHPB**, and (c) **4DBFHPB**. The solid and broken lines indicate the horizontal and vertical components of the optical constants, respectively.

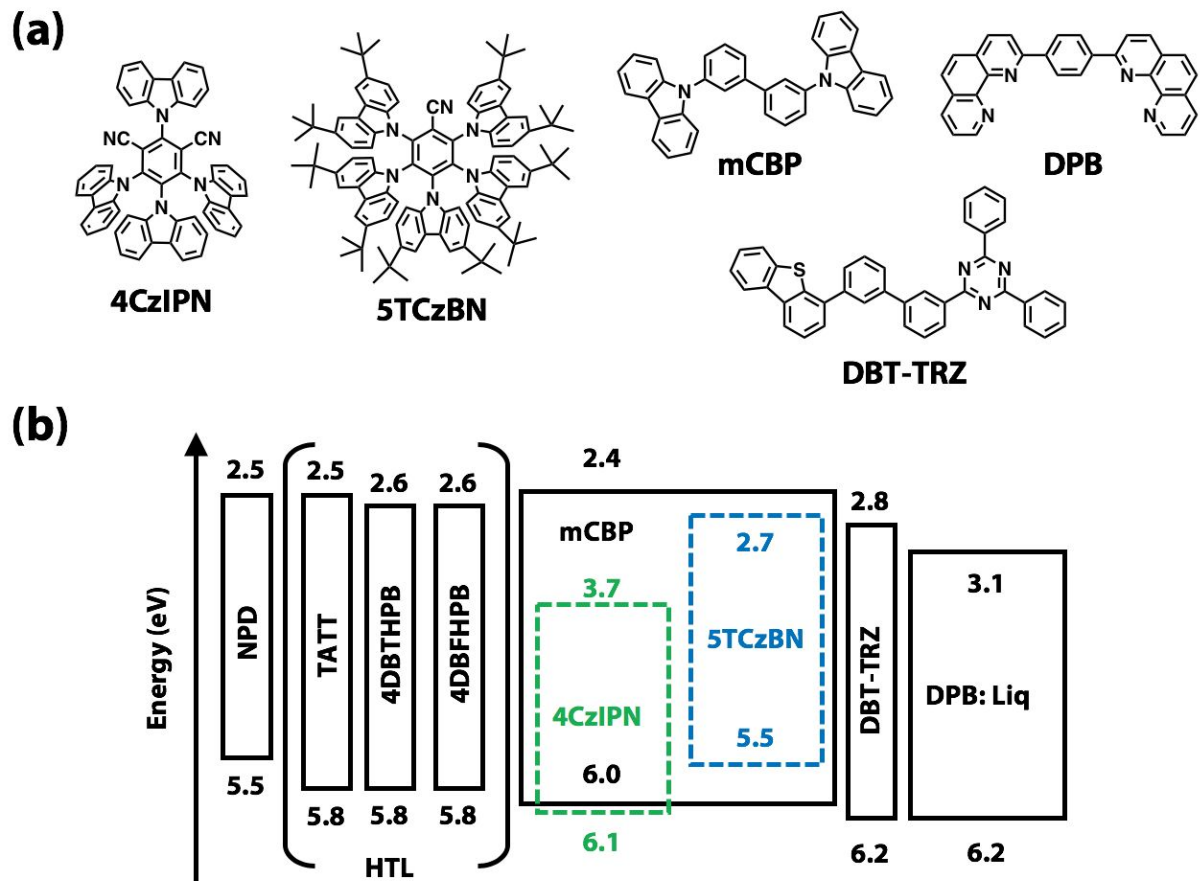


Figure 7. (a) Chemical structures of materials used in OLEDs. (b) Energy diagram of OLEDs.

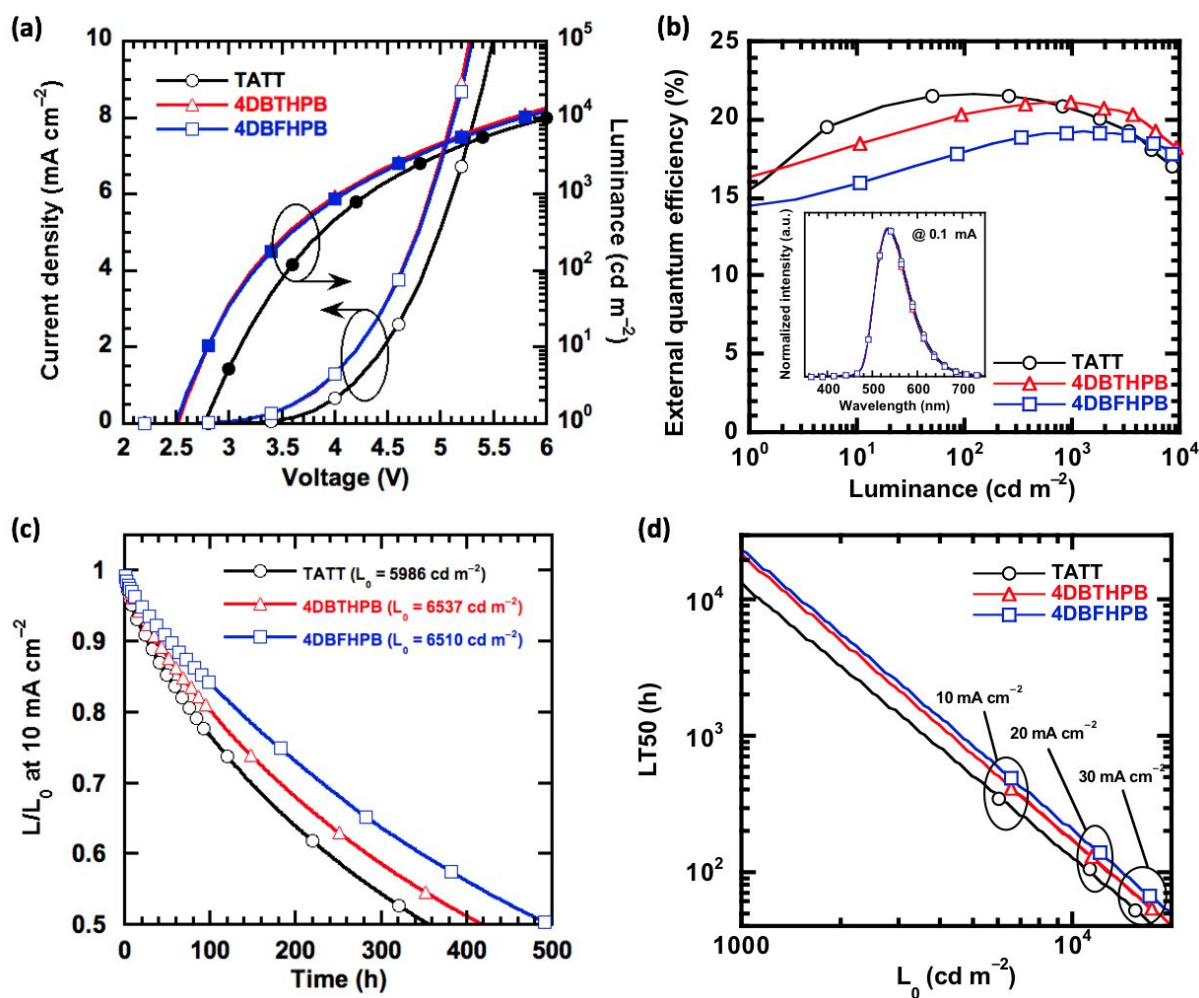


Figure 8. Device performances of green TADF OLEDs: a) J - V - L characteristics, b) η_{ext} - L characteristics, the inset shows EL spectra, c) operation lifetime at 10 mA cm^{-2} , and d) luminance acceleration tests of operation lifetime at 80% of the initial luminance.

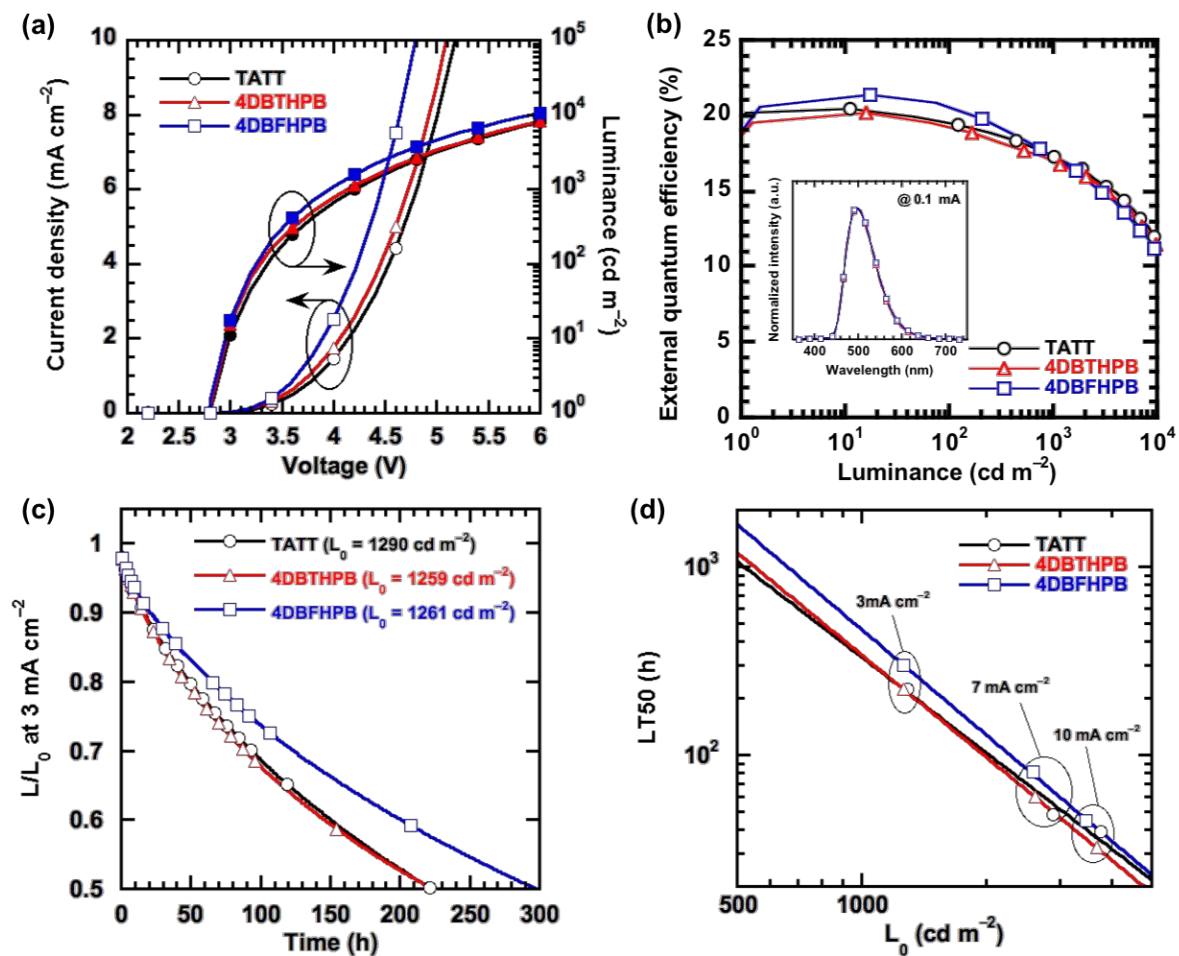


Figure 9. Device performances of sky-blue TADF OLEDs: a) J - V - L characteristics, b) η_{ext} - L characteristics, the inset shows EL spectra, c) operation lifetime at 3 mA cm^{-2} , and d) luminance acceleration tests of operation lifetime at 50% of the initial luminance.

Table 1. Thermal and optical properties.

Compound	Mw	$T_g^a/T_m^a/T_{d5}^b$ (°C)	HOMO ^c /LUMO ^c / E_T^d (eV)	$I_p^e/E_g^f/E_a^g/E_T^h$ (eV)	S^i
TATT	869	194/346/429	-5.17/-1.05/3.02	-5.8/3.4/-2.4/2.7	-0.14
4DBTHPB	1081	146/307/497	-5.24/-1.41/2.82	-5.8/3.2/-2.6/2.7	-0.16
4DBFHPB	1049	135/313/490	-5.20/-1.41/2.78	-5.8/3.2/-2.6/2.7	-0.13

^a T_g and T_m were determined using DSC. ^b T_{d5} was determined using TGA. ^{c,d}Calculated at the RB3LYP 6-311+G(d,p)/RB3LYP 6-31G(d) level. ^dCalculated triplet energy. ^e I_p was determined using PYS. ^f E_g was taken as the point where the normalized absorption spectra intersected. ^g E_a was calculated using I_p and E_g . ^h E_T was estimated from the onset of the phosphorescent spectra at 5 K. ⁱVASE derived order parameter.

Table 2. Hole transport parameters.

Compound	$\mu_h/cm^2 V^{-1} s^{-1}$ [a]	$\mu_0/cm^2 V^{-1} s^{-1}$ [b]	σ/meV [c]	Σ [d]	$C/(cm V)^{1/2}$ [e]
TATT	5.6×10^{-6}	4.1×10^{-4}	96	2.38	3.0×10^{-4}
4DBTHPB	1.5×10^{-3}	1.9×10^{-2}	79	1.45	2.8×10^{-4}
4DBFHPB	1.5×10^{-3}	1.7×10^{-2}	96	1.40	4.0×10^{-4}

[a] Mobility at $5.6 \times 10^5 V cm^{-1}$. [b] Hypothetical mobility in the disorder-free system. [c] Energetic disorder. [d] Positional disorder. [e] Empirical constant.

Table 3. Summary of OLED performances.

Emitter	HTL	V_{on}^a (V)	$V_{1000}/\eta_c, 1000/\eta_p, 1000/\eta_{ext, 1000}^b$ (V/cd A ⁻¹ /lm W ⁻¹ %)	LT ₅₀ at constant current density (h) ^c	LT ₅₀ at 1000 cd m ⁻² (h) ^d	LT ₅₀ at 500 cd m ⁻² (h) ^e
	TATT	2.73	4.30/71.1/52.0/20.8	356	~12,000	~50,000
4CzIPN	4DBTHPB	2.47	4.03/72.7/56.7/21.1	419	~20,000	~90,000
	4DBFHPB	2.45	4.07/66.7/51.5/19.2	497	~24,000	~100,000
	TATT	2.79	4.20/45.5/34.1/17.4	223	~330	~1000
5TCzBN	4DBTHPB	2.76	4.12/44.3/33.8/17.0	224	~340	~1100
	4DBFHPB	2.74	3.94/45.2/36.1/17.3	298	~460	~1700

^a Turn-on voltage at 1 cd m⁻². ^b Voltage, current efficiency (η_c), power efficiency (η_p), and external quantum efficiency (η_{ext}) at 1000 cd m⁻². ^cOperation lifetime at 50% (LT₅₀) of the initial luminance at the constant current density of 10 mA cm⁻² for 4CzIPN-based device, and 3 mA cm⁻² for 5TCzBN-based device. ^dLT₅₀ of 1000 cd m⁻² estimated by luminance acceleration test. ^eLT₅₀ of 500 cd m⁻² estimated by luminance acceleration test.

Table 4. Summary of the performances and the stability in green TADF OLEDs

	Emitter	V_{on}^a (V)	$V_{1000}/\eta_{\text{c},1000}/\eta_{\text{p},1000}/\eta_{\text{ext},1000}^b$ (V/cd A ⁻¹ /lm W ⁻¹ /%)	$\eta_{\text{c,max}}/\eta_{\text{p,max}}/\eta_{\text{ext,max}}^c$ (cd A ⁻¹ /lm W ⁻¹ /%)	LT ₅₀ ^d (h)	LT ₅₀ ^e (h)
This work	4CzIPN	2.45	4.07/66.7/51.5/19.2	72.7/71.3/21.2	860	24,000
Ref. [4a]	4CzIPN	-	-/46.5/28.1/13.9	47.0/30.7/14.0	-	2800
Ref. [4d]	4CzIPN	2.54	4.85/64.0/42.1/19.2	68.3/61.3/20.6	654	10,934
Ref. [4b]	4CzIPN-Me	3.80	6.60/68.0/-/19.7	73.0/-/21.0	-	1472

^a Turn-on voltage at 1 cd m⁻². ^b Voltage, current efficiency (η_{c}), power efficiency (η_{p}), and external quantum efficiency (η_{ext}) at 1000 cd m⁻². ^c Maximum values of voltage, η_{c} , η_{p} , and η_{ext} . ^d Operation lifetime at 50% of the initial luminance of ~5000 cd m⁻². ^e Operation lifetime at 50% of the initial luminance of ~1000 cd m⁻².

Table 5. Summary of the performances and the stability in sky blue TADF OLEDs

	Emitter	V_{on}^a (V)	$V_{1000}/\eta_{\text{c},1000}/\eta_{\text{p},1000}/\eta_{\text{ext},1000}^b$ (V/cd A ⁻¹ /lm W ⁻¹ /%)	$\eta_{\text{c,max}}/\eta_{\text{p,max}}/\eta_{\text{ext,max}}^c$ (cd A ⁻¹ /lm W ⁻¹ /%)	LT ₅₀ ^d (h)	LT ₅₀ ^e (h)
This work	5TCzBN	2.74	3.94/45.2/36.1/17.3	56.1/60.5/21.5	460	1700
Ref. [21]	5TCzBN	2.90	-/-/10.7 ^f	-/56.1/21.2	-	770
Ref. [22]	5TCzBN	3.00	3.90/-/34.1/21.1	-/40.2/21.3	-	475
Ref. [4d]	BCz-TRZ	2.62	5.75/16.8/9.20/7.02	22.5/20.1/8.80	454	-

^a Turn-on voltage at 1 cd m⁻². ^b Voltage, current efficiency (η_{c}), power efficiency (η_{p}), and external quantum efficiency (η_{ext}) at 1000 cd m⁻². ^c Maximum values of voltage, η_{c} , η_{p} , and η_{ext} . ^d Operation lifetime at 50% of the initial luminance of ~1000 cd m⁻². ^e Operation lifetime at 50% of the initial luminance of ~500 cd m⁻². ^f η_{ext} at 500 cd m⁻².

